A Soft, Controllable, High Force Density Linear Brake Utilizing Layer Jamming

Inrak Choi[1], Nick Corson[2], Lizzie Peiros[1], Elliot W. Hawkes[1], Sean Keller[2], and Sean Follmer[1]

***Abstract*—While much work has focused on the design of actuators for inputting energy into robotic systems, less work has been dedicated to devices that remove energy in a controlled manner, especially in the field of soft robotics. Such devices have the potential to significantly modulate the dynamics of a system with very low required input power. In this paper, we leverage the concept of layer jamming, previously used for variable stiffness devices, to create a controllable, high force-density, soft layer jamming brake (SLJB). We introduce the design, modeling, and performance analysis of the SLJB and demonstrate variable tensile resisting forces through the regulation of vacuum pressure. Further, we measure and model the tensile force with respect to different layer materials, vacuum pressures, and lengthening velocities, and show its ability to absorb energy during collisions. We hope to apply the SLJB in a number of applications in wearable technology.**

***Index Terms*—Soft material robotics, wearable robots, hydraulic/pneumatic actuators.**

I. INTRODUCTION

THERE are three main categories of devices that researchers investigate for controlling the dynamics of a robotic system: 1) actuators that create forces to add energy to a system, 2) variable stiffness mechanisms that modulate the form of the energy in the system (e.g. from kinetic to elastic potential energy), and 3) brakes and dampers to remove energy from the system. While many robotic systems rely on traditional actuators like servo motors, researchers have developed artificial muscles to create linear motions with high force density which offer alternatives to motors [1], [2], [3]. Others have focused on designing series elastic actuators or variable stiffness actuators to give compliance during collisions [4], [5], [6]. Finally, the work on energy-removing devices, such as brakes and dampers, includes devices based on varying physics. Researchers have modeled and characterized designs using magnetorheological fluid [7], [8], [9], electrorheological fluid [10], [11], and piezoelectric actuated friction [12]. Other researchers have modeled eddy current brakes [13] and a hydraulic shock absorber [14].

Our focus area within robotics is the relatively new field of soft robotics. Researchers have increasingly investigated soft robotic systems as robots are moving closer to physical interaction with humans in applications such as wearable robotic systems and human-friendly robots [15], [16]. Many soft robotic structures and materials have been investigated for variable stiffness [17], [18], [19]. These new designs are focused on compliance and flexibility for both safety and comfort while attempting to retain the performance found in more rigid systems. While researchers have investigated both soft actuators and soft variable stiffness materials, less research has explored braking in the context of soft robotics.

A soft controllable high force-density brake could be valuable to human-robot interaction and soft robotics. Such a device could have a high force density and low power consumption, capable of improving safety and performance of robotic systems by absorbing mechanical energy. This could have applications especially in wearable robotic systems because a human has hundreds of efficient actuators (muscles) and in many applications, the wearable robotic systems exist for resisting forces between body segments or between the human and the environment outside [20], [21].

Vacuum-controlled jamming is an intriguing technology that has found a number of uses within the robotics community. Here, vacuum pressure is applied to either particles or layers to change the mechanical properties of the system. Researchers have investigated the particle jamming mechanism to utilize its controllable stiffness characteristics for a universal gripper [22], a variable stiffness manipulator [23], a shape-changing display [24], and haptic interface [25], [26], [27]. In the area of layer jamming, Kim et al. designed and evaluated an apparatus using layer jamming for a minimally invasive surgical device [28]. Simon et al. used the layer jamming mechanism for developing a glove-style haptic device [29], and for medical rehabilitation [30]. Ou et al. designed deformable user interfaces enabled by jamming layers [31]. Wall et al. combined both layer and particle jamming units and evaluated their bending force and compressive force before buckling [32].

We believe the mechanism of layer jamming is a viable option for developing a soft controllable brake for robotic and wearable systems. The braking force is set by the friction force, which is controlled by the vacuum pressure applied to the layers. By choosing different materials for layers, and by controlling the vacuuming pressure, we can change the characteristics of the system. A jamming mechanism has the following advantages. First, it can be designed with a high force density. By increasing the number of thin layers, we can increase the contacting surface area, which contributes to the friction force while keeping a compact size and only minimally increasing weight. Second, the jamming mechanism is safe

Manuscript received: June, 18, 2017; Revised September, 1, 2017; Accepted September, 27, 2017.

This paper was recommended for publication by Editor Yu Sun upon evaluation of the Associate Editor and Reviewers' comments. *This work was supported in part by Oculus VR, LLC and Stanford University

[1]The Department of Mechanical Engineering at Stanford University, 450 Serra Mall, Stanford, CA 94305, USA {irchoi, epeiros, ewhawkes, sfollmer}@stanford.edu

[2]Oculus VR, LLC, Redmond, WA 98052 USA {nick.corson, sean.keller}@oculus.com

Digital Object Identifier (DOI): see top of this page.

This article has been accepted for publication in a future issue of this journal, but has not been fully edited. Content may change prior to final publication. Citation information: DOI 10.1109/LRA.2017.2761938, IEEE Robotics and Automation Letters

and comfortable for use in contact with humans. Third, the jamming mechanism is controlled via pressure, with pumps external to the site of actuation. Therefore, the device does not require local electric and magnetic fields and is thus MR-compatible. However, there are some limitations of the jamming mechanism. Most notably, the controllable pressure range is only from atmospheric pressure to vacuum, which is a narrower bandwidth than positive pressure pneumatic systems.

This paper explores the energy removal characteristics of layer jamming in the longitudinal (i.e. tensile) direction. We first introduce a dynamic model for simulating its tensile force with respect to linear displacement. Next we present experimental results, validating the model as well as testing the soft layer jamming brake (SLJB) while varying factors such as the material of the layers, the working fluid, the vacuum pressures, and the pulling speeds. Finally, we test the controllable braking capability with a simple drop test in which the SLJB greatly reduces the accelerations felt by the falling object when it is stopped.

II. METHODS AND MODELS

A. Structure of the SLJB

A SLJB unit consists of n layers of stacked material split evenly for attachment to two opposite endcaps, endcap right and endcap left. There is a length L_1, which is the length protruding from the left endcap that does not overlap with the layers from the right. Then a length L_2 that corresponds to the length of the overlapping region and a length L_3 for the length over which the layers protruding from the right do not overlap with the left layers. Each of these regions also has a corresponding area, A_1, A_2, A_3 as designated by the length L_n and the chosen uniform width of the layers. The layers and housing also have a thickness t_{layer} and t_{housing}. The housing as well can be made from different stiffness of material. The assembly of these materials is as follows: connect the layers to the two end caps and fasten down with corresponding screw, interleaving the left and right layers, sliding on the enclosure and zip-tying it onto the endcaps.

As shown in Fig.1, each SLJB consists of 11 layers of material stacked one on top of the other, 2 end caps, a flexible outer enclosure, tube fittings and fasteners and zip-ties to hold the mechanism together. The layers are split in half and anchored into either the left or right side of the unit seen in the CAD model shown in Fig. 1. The selected layer material, specifically the relevant coefficients of friction as well as the elastic properties, affect the overall performance of the SLJB while under tension in the jammed state. Each layer has 0.254 mm thickness, 13 mm width, and 85 mm length. We cut the layers using a CO2 laser cutter.

The two end caps are 3D-printed in a plastic material using SLA manufacturing techniques. The elastic modulus of the material is 2.5 GPa. These two anchors also have ports, where the tube fittings are fixed, which allow for an exchange of fluids, air or water.

The flexible outer cover is made from ecoflex 5 platinum catalyzed silicon that is zip tied to each anchor to form an air/water tight seal. The 100% elastic modulus is 0.1 MPa

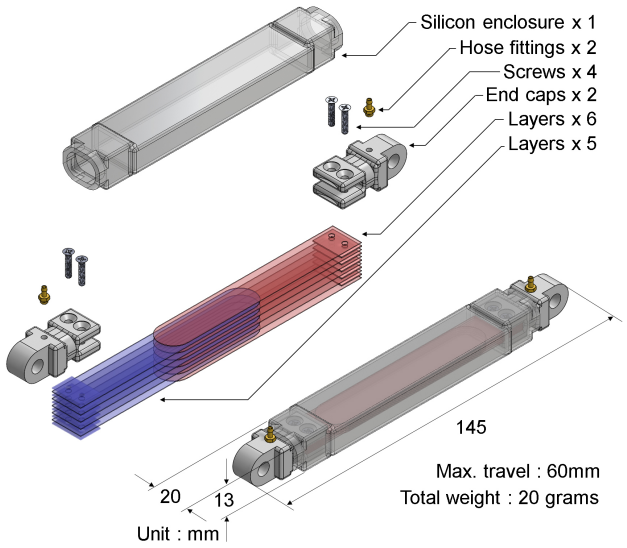

Fig. 1. Components and geometry of the SLJB. *From top left*: 1) Outer housing made from a silicone material. 2) Fasteners and tube fittings that allow for intake and removal of air from the jammer. 3) End caps onto which all other elements are fixtured followed by. 4) Jamming sheets layered together from opposite sides. 5) Full assembly showing how the elements fit together. The number of layers and dimensions can be modified based on the required specifications.

and the wall thickness is 1 mm. To create the silicone part, an injection mould was created with 3D printing, then a dispenser was used to mix the two part silicone cure then press it into the mold to form the desired shape and avoid bubble formation.

The overlapped length between left and right layers is 68 mm at the default configuration (relaxed state), so it can be stretched up to about 60 mm leaving 8mm of overlap. However, in our experimental testing the SLJB did not exceed 40mm of displacement. The total weight of each unit is about 20 grams.

The current SLJB design works only in tensile motion. If the SLJB is in compression, buckling will occur because it is composed of thin layers. To use the SLJB in both directions, two SLJBs and a pulley are required for antagonistic pairs.

B. Model

To model the SLJB we begin with a simplification of the actual system into a representative system. Fig. 2 (a) shows the actual system and all relevant forces to our simulation. Fig. 2 (b) shows a static model when the SLJB is loaded in tension but the layers have not started sliding yet. In this case, the SLJB acts like a series of springs. Fig. 2 (c) shows a simple dynamic model when the SLJB is sliding. This is represented by a block connected with two springs one on each side and pulled to the right. There are external forces on the block to the left, which oppose the tensile force, equal to the summation of f_f and f_e.

1) Before the layers start sliding (Fig.2(b)): When the tensile strength is smaller than the static friction force between layers, the SLJB will act like a stiff spring and stores mechanical energy. This region should be minimized for a larger range of controllable displacement to use the SLJB as a brake. In Fig. 2 (a) we can see 3 distinct sections of layering: layers

This article has been accepted for publication in a future issue of this journal, but has not been fully edited. Content may change prior to final publication. Citation information: DOI 10.1109/LRA.2017.2761938, IEEE Robotics and Automation Letters

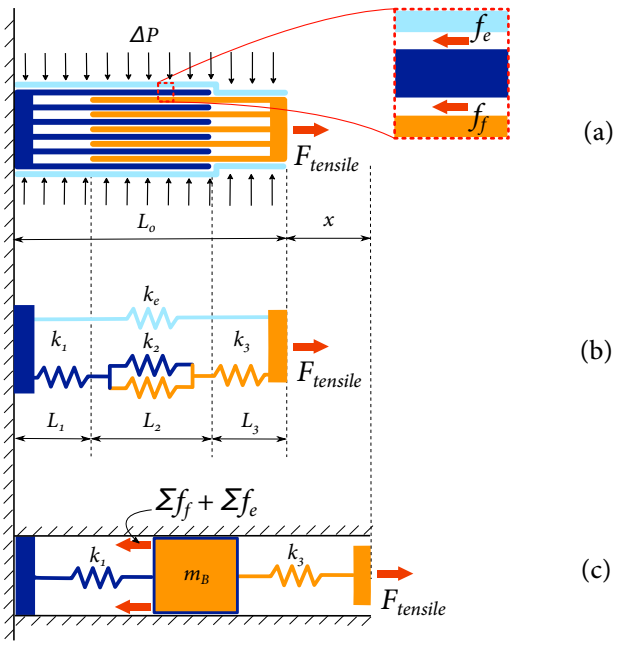

Fig. 2. 1-D free-body diagram of SLJB when it is jammed. The blue part is grounded, and the yellow part slides. (a) A schematic of the SLJB, showing a jammed state with an external lateral force, $F_{tensile}$. The forces that oppose this force in the SLJB, the elastic force f_e (force due to the interactions between the silicone housing and the sheet layers) and the friction force f_f (force due to friction between layers) are shown with dashed lines circling them. (b) A static model when the SLJB is jammed and being pulled and did not start to slide yet. (c) A dynamic model when the SLJB is jammed and pulled, and sliding. The SLJB is represented by a block, which encompasses the mass and motion of the jamming layers relative to one another, forces F_f and F_e, which represent the interaction forces between layers and between the layers and housing, and the rigid body is connected with two springs, which represent the stiffness of the layered materials.

from the left (blue), layers from the right (orange), and layers from the right and left stacked together (blue and orange). Since each section has a different number of layers, we chose to model each separately as a spring leaving the SLJB as a set of 3 springs in series (shown in Fig. 2 (b)). Therefore, the tensile force in the static case can be described as below.

$$F_{tensile} = k_{effective}x = (1/k_1 + 1/k_2 + 1/k_3)^{-1}x \quad (1)$$

where

$$k_i = E_l A_i / L_i (i = 1,2,3) \quad (2)$$

where $k_{effective}$ is the net spring constant of three springs, E_l is the tensile modulus of the layer material, L_i and A_i are the length and cross-sectional area of each stack of layers.

2) Once the layers start to slide (Fig.2(c)): When the tensile strength exceeds the static friction force between layers, layers start to slide and they absorb mechanical energy. Our model changes to where the friction force between layers and spring force from the elastic enclosure generate the force. Then the block in our model in Fig. 2(c) will receive the following amount of force from the enclosure and layers (Note that Eq.5 was derived in detail in a previous work [28] and has been slightly modified for this application). The equation shown below has been modified based on our specific modelling assumptions. First we took into account that two sides of the device are actively creating the F_e force. The top and bottom

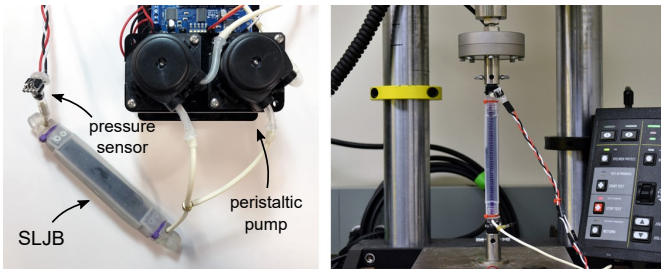

Fig. 3. Pressure controller composed of a pressure sensor and peristaltic pumps (left), and tensile testing setup using Instron 5848 Microtester (right)

have significant contact with the enclosure while the sides have negligible contact meaning the original equation is doubled to take into account our modeling assumptions.

$$F = F_f + F_e = \sum_{1}^{n-1} f_f + \sum_{1}^{2} f_e \quad (3)$$

where

$$F_f = \mu(n-1)W(L_2 - x)\Delta P \quad (4)$$

and

$$F_e = 2\sqrt{E_e A_e \Delta P \mu_e W x} \quad (5)$$

The block will be pulled by two springs and the effective spring constant, $k_{effective}$, is

$$k_{effective} = (1/k_1 + 1/k_3)^{-1} \quad (6)$$

C. Test Setup and Experiment Procedure

To measure the tensile force of the SLJB, we used an Instron 5848 MicroTester and a 500N load cell with a 1000 Hz sampling rate.

Each end cap was designed such that it can easily be attached to the Instron machine for accurate and repeatable results. They were made such that each could be fixed using a dowel pin insert of 6 mm in diameter to ensure a close slip-fit to minimize slop, but allow for ease of assembly. Once the module was connected on both ends and before any experiments were run, a short calibration for the load cell was used. During the experiment, the valve connected to the air pump was pre-set with a controller to maintain a constant set pressure. As shown in Fig.3 (right), the tubing was connected to the base which on the machine is stationary. The pressure sensor was connected at the top port, which is on the opposite side from the tubing so that we can guarantee the entire area inside has correct vacuuming pressure.

To control the vacuuming pressure, we used peristaltic pumps for actuation and Honeywell 24PCCFB6G sensors for sensing pressure. The pressure controller in Fig. 3 (left) was small and light enough to carry to the testing room, but also suitable to use in both pneumatic and hydraulic conditions. However, the flow rate was low so we connected two peristaltic pumps in parallel and the maximum flow rate was 3.33 mL/s.

This article has been accepted for publication in a future issue of this journal, but has not been fully edited. Content may change prior to final publication. Citation information: DOI 10.1109/LRA.2017.2761938, IEEE Robotics and Automation Letters

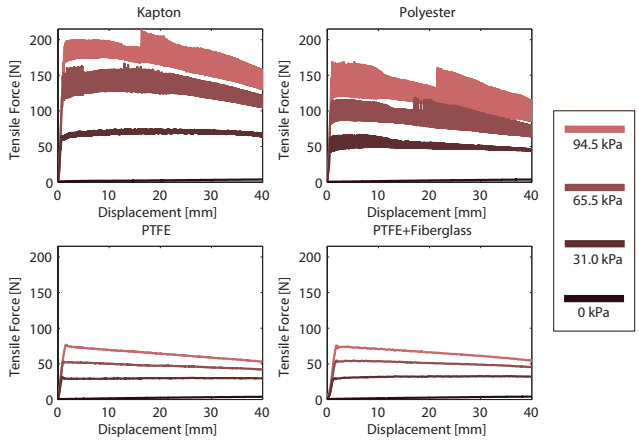

Fig. 4. Tensile testing results using four materials (Kapton, Ployester, PTFE, PTFE+Fiberglass) with 1mm/s pulling speed. Tests were conducted at four vacuuming pressures: 94.5, 65.5, 31.0, and 0 (atmospheric) kPa.

III. EXPERIMENTAL RESULTS

A. Exploration of Different Layer Materials

To investigate the differences between layer materials, we picked four materials: Kapton, polyester, PTFE, and fiberglass with PTFE coating. Each material was tested separately, with 11 interdigitated layers inserted into a different SLJB for each material. For each vacuuming pressure, each material was measured once at 1mm/s pulling speed.

Fig. 4 shows the tensile testing results. By looking general trends, force curves in high vacuuming pressure have negative slopes as the contact area decreases with elongation. In lower vacuuming pressure, the slopes become positive. This shows that the friction force is more dominant than the elastic force in high vacuuming pressure, and the elastic force is more dominant than the friction force in low vacuuming pressure.

Among four materials, Kapton has the largest tensile force and PTFE the smallest. Also, at this slow pulling speed, the force curves of Kapton and polyester have large vibrations while PTFE and Fiberglass with PTFE coating have negligible vibrations. We hypothesis this noise is caused by stick-slip motion; As the friction force changes during the transition between static and kinetic states, the layers repeatedly stop and start moving. Mitiguy et al. showed an algorithm to simulate this motion [33]. In this work, we do not simulate the stick-slip motion because it occurred only in slow pulling speeds. However, it will be relevant to investigate how to minimize it in future work.

Based on this initial testing, we decided to use Kapton and PTFE materials for our experiment and simulation. This is because Kapton has the highest tensile force and less stick-slip motion than polyester, and PTFE exhibited very small stick-slip motion even though it has small tensile force scale.

B. Pneumatic and Hydraulic Actuation

Researchers have used pneumatic or hydraulic actuation for jamming systems. To understand differences, we compared pneumatic and hydraulic actuation with the SLJB. First, we compared the actuation speed using the same peristaltic pump. The desired vacuuming pressure was set to 94.5 kPa, and the

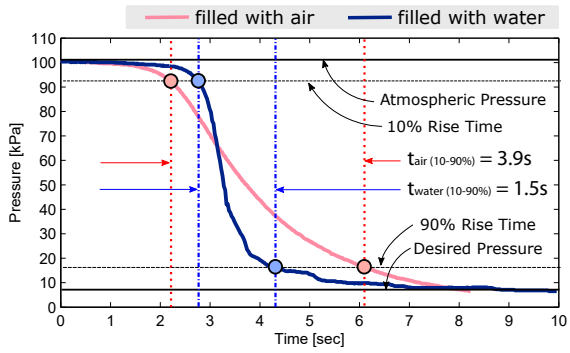

Fig. 5. Step response comparison between air and water fluid actuation looking at rise time (10% - 90%) to our desired vacuum pressure (94.5 kPa).

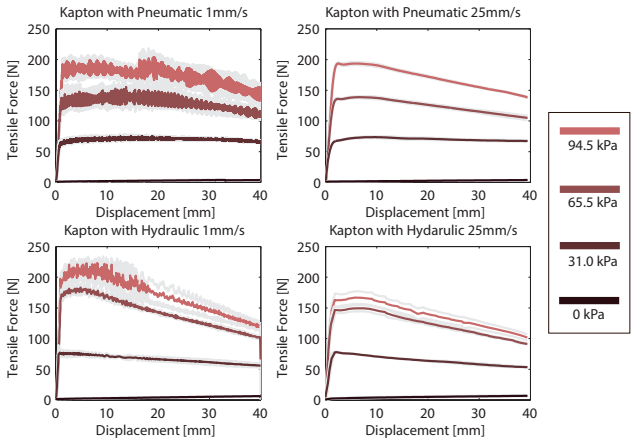

Fig. 6. Tensile results using Kapton in air and fluid with four vacuuming pressures (94.5, 65.5, 31.0, 0 kPa). Light grey lines show one standard deviation error respectively.

SLJB was not under tension or moving at this time. For the hydraulic actuation condition, we filled the inside of the SLJB and tubing with water by circulating water through two tube fittings until all air was flushed out of the system. Fig. 5 shows the step responses of the pneumatic and hydraulic conditions. We measured the 10% - 90% rise times of pneumatic and hydraulic actuation. The response times were 3.9 s and 1.5 s respectively. The hydraulic system had a 2.6 times faster response time than pneumatic due to water's incompressibility.

Secondly, we investigated the tensile force performance. In this test, we chose to use Kapton to compare performance. The SLJB was pulled with 1mm/s and 25mm/s speeds for both conditions and measured three times per pressure. For this experiment we used four vacuuming pressures, 94.5 kPa, 65.5 kPa, 31.0 kPa, and 0 kPa. Fig. 6 shows the results, with one standard deviation in error (light gray lines).

Under the dry condition, the tensile force was not affected by pulling speeds. This shows the tensile force is dominated by Coulomb friction and the behavior is quasi-static. Under the wet condition, the tensile force was affected by pulling speeds. The peak force in wet conditions at low speed was higher than under dry conditions. Conversely, the peak force at high speed was lower in dry conditions than in wet conditions. Also, the slope of the force curve in wet conditions was more steep compared to the curve in dry conditions.

Based on the comparisons between the pneumatic and

This article has been accepted for publication in a future issue of this journal, but has not been fully edited. Content may change prior to final publication. Citation information: DOI 10.1109/LRA.2017.2761938, IEEE Robotics and Automation Letters

TABLE I
EXPERIMENTAL FRICTION COEFFICIENTS IN DRY CONDITIONS.

Material	Friction Coefficient		Standard Deviation Error	
	static	kinetic	static	kinetic
Kapton	0.32	0.24	8.18%	2.77%
PTFE	0.12	0.05	8.71%	3.17%

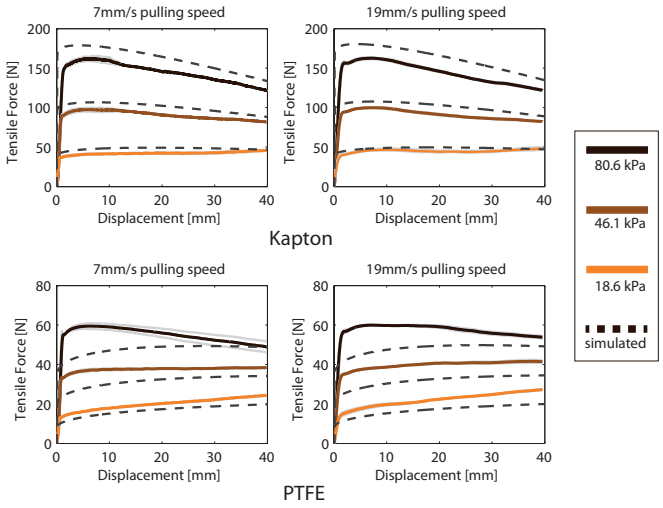

Fig. 7. Simulation model validation with experimental results at 80.6, 46.1, 18.6 kPa vacuuming pressures. Light grey lines show one standard deviation error respectively. Dashed lines are corresponding simulation results. Simulation is done based on the dynamic model in Fig.2(c).

hydraulic actuation, we decided to use the pneumatic system. Although the hydraulic actuation created a faster response time, the tensile force behavior in the wet condition was harder to model due to the effects of adhesion and lubrication. In addition, the tensile force in the dry condition tends to be quasi-static making it easier to model.

C. Model Validation

Obtaining correct friction coefficients is important for simulation because friction dominates the overall performances of the SLJB. To measure friction coefficients of materials, we built a custom friction test rig based on ASTM D1894-14, a standard test method for static and kinetic coefficients of friction of plastic film [34]. The set up consisted of a pulley system connected to the Instron and a known weight glued to a thin layer of a material of interest. The weight was then pulled by the Instron causing the weight to slide across a second thin layer of the same material to collect data on static and kinetic friction between the jammed layers shown in figure 3(b). The pulling speed was 2.5 mm/s as the standard test method suggests. The travel was 100 mm. The sliding material had 25 * 25 mm^2 contact area and the weight for normal force was 250 g. Each material was measured three times each in dry and wet conditions. The maximum friction force was selected to calculate the static friction force, and the average force between 40-100 mm was used selected to calculate the kinetic friction force. Finally, the average value of three measurements is used for the representative friction coefficient. Table I shows the friction coefficients of each material with respect to itself.

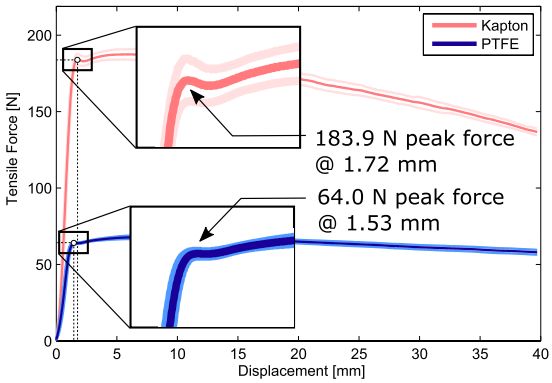

Fig. 8. Tensile experiments to calibrate Kapton and PTFE at 94.5 kPa vacuuming pressure and 13mm/s pulling speed. Based on the forces and displacements at the peaks, the effective stiffness is 107 N/mm and 42 N/mm, and the scale factor for calibration is 0.875 and 1.24 respectively.

The friction coefficients of the silicon material with respect to kapton and PTFE was 0.80 and 0.23 respectively.

To validate the dynamic model, our code was simulated via MotionGenesis software and C. For simulation data, we used kinetic friction coefficients for the entire motion, and did not use static friction coefficients. This is because the layers in a SLJB slide at slightly different times from one another. For the experimental data, we conducted tensile tests using the pneumatic control system as described earlier in this paper. These tensile tests were done at different sets of vacuuming pressures and pulling speeds. The vacuuming pressures were 80.6 kPa, 46.1 kPa, and 18.6 kPa, and the pulling speeds were 7 mm/s and 19 mm/s. Each condition was measured three times.

Fig. 7 shows the results. The simulation data are overlaid in dashed lines on top of the experimental results. The average of mean absolute percentage errors (MAPE) between simulation and experimental curves was 32% on average from the 12 cases and standard deviation of the average was 11%.

D. Calibration

In this section, we introduce how to calibrate the dynamic model for more reliable simulation. While there could be many sources of error, we only focus on the errors from the friction force calculation, F_f, because it is the most significant contributor to the tensile force. The following annotates some of causes of error in our calculated F_f and the actual F_f in our real system:

- A coefficient of friction, although generally modeled as constant, is slightly different with respect to normal pressures applied. The standard test method (ASTM D1894-14) uses only 3.9 kPa (250g weight with 25 * 25 mm^2 contact area) of normal pressure while the SLJB is controlled in between 0 and 101.3 kPa.
- A coefficient of friction is influenced by not only material properties but also the surface condition of layers. The condition of layers might change after assembling and after multiple cycles of use.
- The actual contact area among layers is likely not exactly our calculated contact area, which assumes perfect alignment of the layers.

This article has been accepted for publication in a future issue of this journal, but has not been fully edited. Content may change prior to final publication. Citation information: DOI 10.1109/LRA.2017.2761938, IEEE Robotics and Automation Letters

To compensate for these errors ascribed to F_f, we embedded a scaling factor, a, into our equation for F_f to better align with what we saw experimentally from the system, as shown in Eq.7.

$$F_{f_{calibrated}} = a * F_f \tag{7}$$

To calculate the scale factor, a, we started by implementing one tensile test for each layer material. The results are shown in Fig.8. There is an initial peak which denotes the time at which all layers lose contact. The region that follows can be associated with the linear loss of contact area. Assuming the model of F_e is correct, this term contributes very minimally to tensile force at this small displacement. Therefore, we know all the values of constants and variables in Eq.3 except a (Eq.8) our variable of interest we wish to solve for.

$$a = \frac{F_{peak} - F_e}{F_f} = \frac{F_{peak} - 2\sqrt{E_e A_e \Delta P \mu_e W d_{peak}}}{\mu_k (n-1) W (L_2 - d_{peak}) \Delta P} \tag{8}$$

The a of Kapton and PTFE are 0.875 and 1.24 respectively.

We can also get experimental effective stiffness from Fig. 8 using Eq.9.

$$k_{effective} = F_{peak} / d_{peak} \tag{9}$$

The stiffness measured are 131 kN/m and 55 kN/m for Kapton and PTFE respectively. These are much lower than the values initially calculated using Eq. 6, which are 2050 kN/m and 410 kN/m respectively. This difference comes from the structure of the end caps and mounting parts. To mount the SLJB to the Instron machine, 3d-printed adapter were hooked with dowel pins.

Fig. 9 shows the simulation results after the calibration. The average of MAPEs between simulation and experimental curves was 7.2% and standard deviation of the average was 3.7%.

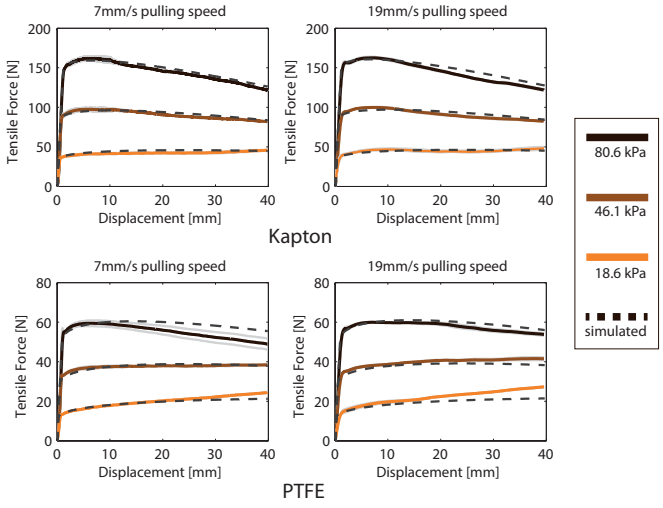

Fig. 9. Simulation model validation after considering errors by multiplying the scaling factor a at 80.6, 46.1, 18.6 kPa vacuuming pressures. Light grey lines show one standard deviation error respectively. Dashed lines are corresponding simulation results.

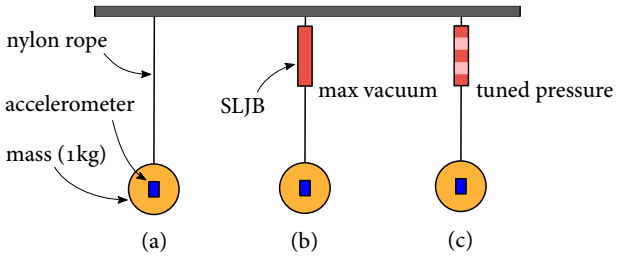

Fig. 10. Damping test setup. A 1kg mass free falls and an accelerometer measures the max acceleration. Conducted in different conditions. (a) without the SLJB. (b) The SLJB is vacuumed maximum (c) The SLJB is vacuumed to an tuned pressures ensuring the 40mm travel.

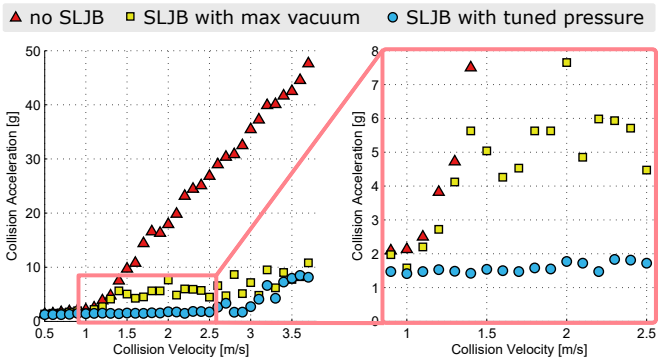

Fig. 11. Damping test result. No SLJB (triangle) leads to a higher peak acceleration for a given velocity. The SLJB with max pressure(square) has a much better performance. The SLJB with tuned pressure (circle) performed even better from slower velocities.

E. Damping Performance

As we now have a reliable tensile force model, we can use the SLJB not only as a brake but also a damper. Assuming the elastic behavior before the layers slide is very small, we can calculate the energy dissipated by the SLJB during 40 mm of travel. Designing the travel distance, the dissipated energy by SLJB is a function of vacuuming pressure.

$$E_{dissipated}(\Delta P) = \int F_{tensile}(x, \Delta P) dx \approx \int_0^{0.04} (F_f(x, \Delta P) + F_e(x, \Delta P)) dx \tag{10}$$

We tested damping performances of the SLJB and Fig. 10 shows the test setup. It is an acceleration-measuring test during free falls. A 1kg mass was tied to a nylon rope. An accelerometer, ADXL193 (Analog Devices), was attached to the mass to measure the maximum acceleration during collision. Then we calculated the velocity just before collision and the kinetic energy based on the dropping height of the mass.

The experiment was done in three conditions: without the SLJB, with the SLJB vacuumed maximum, and with the SLJB having a tuned vacuuming pressure based on Eq. 10 guaranteeing the travel is always 40 mm. The reason we divided the experiment into two modes (maximum pressure and tuned pressure) is that in some conditions we can predict kinetic energy of a system in real time, but sometimes we

This article has been accepted for publication in a future issue of this journal, but has not been fully edited. Content may change prior to final publication. Citation information: DOI 10.1109/LRA.2017.2761938, IEEE Robotics and Automation Letters

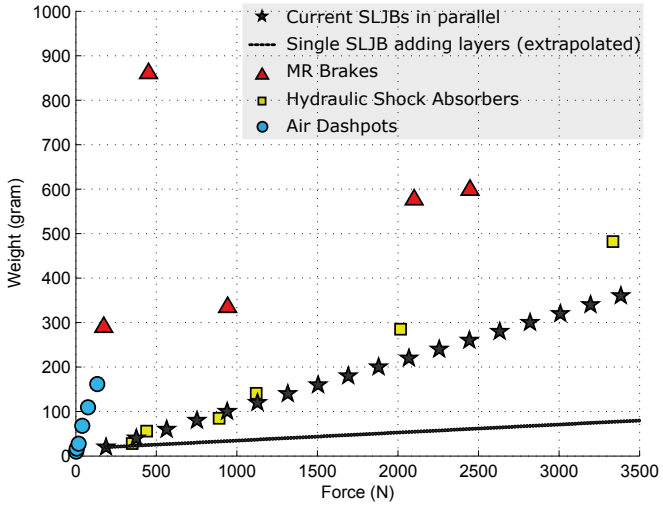

Fig. 12. Force density (weight-force ratio) comparisons among SLJB, MR brakes, hydraulic shock absorbers, and air dashpots.

cannot due to the absence of a valid sensor or a slow actuation speed.

Fig. 11 shows the damping test results. Without the SLJB, a pure nylon rope generated a maximum acceleration up to 50g (50 times of acceleration of gravity) at the 3.7 m/s collision speed. With the SLJB maximumly vacuumed, the SLJB absorbed significant amount of kinetic energy by deforming the length. The collision acceleration decreased to roughly 20 % of the no SLJB drop test results. With the SLJB controlled to the calculated ideal pressure, the acceleration decreased even more significantly. The acceleration does not exceed over 2g until 2.5 m/s speed.

F. Force Density

One of the strengths of jamming mechanism is that the brake mechanism (separate from an external pump) is very compact and light-weight yet provides high resisting force. Fig. 12 compares the force density of various linear dampers.

The weight of MR brakes was calculated based on the MR-fluid volume of each brake by multiplying it with a known density of MR fluid ($3.5g/cm^3$). The volume information of MR brakes was available in the work of Alkan et al [8]. Commercial products were chosen for hydraulic shock absorbers (ITT Enidine Inc.) and air dashpots (Airpot Corporation).

The SLJB (with Kapton) has the largest force-weight ratio among the four brakes. The star-shape plot shows when we add the current SLJB design in parallel. The dashed line shows the extrapolated performance when we just add layers in a single SLJB. By adding one more layer we can increase 17.5 N while the weight is increased 0.4 grams. This force density can increase even more if the Kapton surface is treated to increase the friction coefficient. Selecting different materials having higher friction coefficients is another option to increase the force density.

IV. CONCLUSION AND FUTURE WORK

In this paper, we designed and investigated a linear brake using layer jamming, called a SLJB. We provided a model

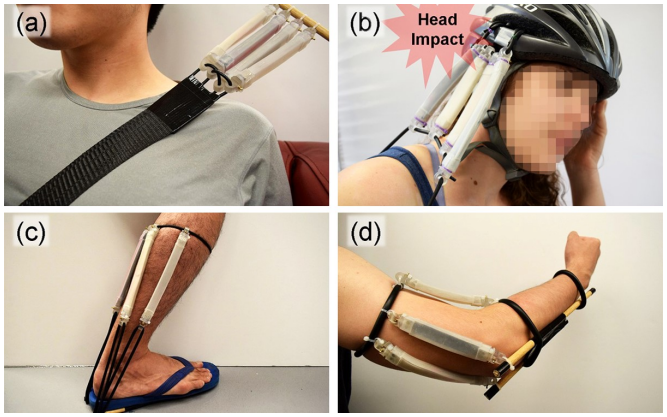

Fig. 13. Possible applications of SLJB. (a) damping seat belt (as a damper) (b) damping neck guard connected with a helmet (as a damper) (c) ankle exoskeleton (as a clutch) (d) flexion muscle rehabilitation (as a brake)

that gives an accurate curve for tensile force with input vacuum pressure and travel distance, and described the SLJB capabilities to function as a variable damper to maximize energy dissipation for a given system. Before modeling we showed the pros and cons to certain material choices (high force with noise, lower force with no noise) and activating fluid (less model complications in air, faster response time in water). Based on these experiments we chose to use PTFE and Kapton to model the transfer function from our input, pressure, to our output, tensile force. Once we were able to achieve this model we could reasonably predict the results for experiments with different pulling speeds and pressures. This information was then used to calculate a pressure to maximize energy dissipation in our drop test. In that test we proved that a calibrated SLJB outperformed a maximally active SLJB and both performed far better than the string.

The SLJB can be adapted to soft wearable robotic systems as a damper, brake or clutch. We roughly prototyped some SLJB applications to show its use in the future. Fig. 13 (a) and (b) show the SLJB used as a damper. As shown in (a), by attaching SLJBs to a seat belt in series, we can make a compact damping seat belt to absorb the driver's kinetic energy in a collision. Fig. 13 (b) shows an active damping neck guard. There are a number of head injuries in football games and one of the main reason is a human's head experiences extreme acceleration when there is a head collision (researchers have measured that peak angular acceleration is over 3500 rad/s^2 during a head impact with a football helmet [35]). By connecting the helmet and neck guard with SLJBs, we expect it significantly decreases the collision acceleration. Fig. 13 (c) shows the SLJB used as a clutch. Researchers developed a lightweight ankle exoskeleton using a electrostatic clutch and a spring [36]. The electrostatic clutches could be replaced with SLJBs with a more compact size for same braking force. The recovering force will be generated from the rubber tubes passively and the SLJB would act like clutches unless the tensile force is stronger than the SLJB's maximum force. Researchers have applied brake mechanisms into muscle exercise machines for rehabilitation [37], [38], [11]. Other researchers have proposed layer jamming mechanism

for medical rehabilitation [30]. The SLJB can be also used as a brake in wearable rehabilitation devices as shown in (d).

ACKNOWLEDGMENT

We thank Marc Levenston for offering the Instron machine. We also thank Adam W. Caccavale for helping preliminary tensile testing and friction measurement.

REFERENCES

[1] B. Tondu and P. Lopez, "Modeling and control of mckibben artificial muscle robot actuators," *IEEE control systems*, vol. 20, no. 2, pp. 15–38, 2000.

[2] C. S. Haines, M. D. Lima, N. Li, G. M. Spinks, J. Foroughi, J. D. Madden, S. H. Kim, S. Fang, M. J. de Andrade, F. Göktepe, *et al.*, "Artificial muscles from fishing line and sewing thread," *science*, vol. 343, no. 6173, pp. 868–872, 2014.

[3] E. W. Hawkes, D. L. Christensen, and A. M. Okamura, "Design and implementation of a 300% strain soft artificial muscle," in *Robotics and Automation (ICRA), 2016 IEEE International Conference on*. IEEE, 2016, pp. 4022–4029.

[4] G. A. Pratt and M. M. Williamson, "Series elastic actuators," in *Intelligent Robots and Systems 95.'Human Robot Interaction and Cooperative Robots', Proceedings. 1995 IEEE/RSJ International Conference on*, vol. 1. IEEE, 1995, pp. 399–406.

[5] B. Vanderborght, A. Albu-Schäffer, A. Bicchi, E. Burdet, D. G. Caldwell, R. Carloni, M. Catalano, O. Eiberger, W. Friedl, G. Ganesh, *et al.*, "Variable impedance actuators: A review," *Robotics and autonomous systems*, vol. 61, no. 12, pp. 1601–1614, 2013.

[6] S. Wolf, G. Grioli, O. Eiberger, W. Friedl, M. Grebenstein, H. Höppner, E. Burdet, D. G. Caldwell, R. Carloni, M. G. Catalano, *et al.*, "Variable stiffness actuators: Review on design and components," *IEEE/ASME transactions on mechatronics*, vol. 21, no. 5, pp. 2418–2430, 2016.

[7] J. D. Carlson and M. R. Jolly, "Mr fluid, foam and elastomer devices," *mechatronics*, vol. 10, no. 4, pp. 555–569, 2000.

[8] M. S. Alkan, H. Gurocak, and B. Gonenc, "Linear magnetorheological brake with serpentine flux path as a high force and low off-state friction actuator for haptics," *Journal of Intelligent Material Systems and Structures*, vol. 24, no. 14, pp. 1699–1713, 2013.

[9] H.-U. Oh and J. Onoda, "An experimental study of a semiactive magneto-rheological fluid variable damper for vibration suppression of truss structures," *Smart Materials and Structures*, vol. 11, no. 1, p. 156, 2002.

[10] N. K. Petek, "An electronically controlled shock absorber using electrorheological fluid," SAE Technical Paper, Tech. Rep., 1992.

[11] J. Nikitczuk, B. Weinberg, P. K. Canavan, and C. Mavroidis, "Active knee rehabilitation orthotic device with variable damping characteristics implemented via an electrorheological fluid," *IEEE/ASME transactions on Mechatronics*, vol. 15, no. 6, pp. 952–960, 2010.

[12] M. Laffranchi, N. G. Tsagarakis, and D. G. Caldwell, "A variable physical damping actuator (vpda) for compliant robotic joints," in *Robotics and Automation (ICRA), 2010 IEEE International Conference on*. IEEE, 2010, pp. 1668–1674.

[13] J. Edwards, B. Jayawant, W. Dawson, and D. Wright, "Permanent-magnet linear eddy-current brake with a nonmagnetic reaction plate," *IEE Proceedings-Electric Power Applications*, vol. 146, no. 6, pp. 627–631, 1999.

[14] S. Duym, R. Stiens, and K. Reybrouck, "Evaluation of shock absorber models," *Vehicle system dynamics*, vol. 27, no. 2, pp. 109–127, 1997.

[15] D. Rus and M. T. Tolley, "Design, fabrication and control of soft robots," *Nature*, vol. 521, no. 7553, pp. 467–475, 2015.

[16] D. Shin, I. Sardellitti, Y.-L. Park, O. Khatib, and M. Cutkosky, "Design and control of a bio-inspired human-friendly robot," *The International Journal of Robotics Research*, vol. 29, no. 5, pp. 571–584, 2010.

[17] C. Majidi and R. J. Wood, "Tunable elastic stiffness with microconfined magnetorheological domains at low magnetic field," *Applied Physics Letters*, vol. 97, no. 16, p. 164104, 2010.

[18] W. Shan, T. Lu, and C. Majidi, "Soft-matter composites with electrically tunable elastic rigidity," *Smart Materials and Structures*, vol. 22, no. 8, p. 085005, 2013.

[19] A. Firouzeh, M. Salerno, and J. Paik, "Soft pneumatic actuator with adjustable stiffness layers for multi-dof actuation," in *Intelligent Robots and Systems (IROS), 2015 IEEE/RSJ International Conference on*. IEEE, 2015, pp. 1117–1124.

[20] C. J. Walsh, K. Endo, and H. Herr, "A quasi-passive leg exoskeleton for load-carrying augmentation," *International Journal of Humanoid Robotics*, vol. 4, no. 03, pp. 487–506, 2007.

[21] W. Van Dijk, H. Van der Kooij, and E. Hekman, "A passive exoskeleton with artificial tendons: Design and experimental evaluation," in *Rehabilitation Robotics (ICORR), 2011 IEEE International Conference on*. IEEE, 2011, pp. 1–6.

[22] E. Brown, N. Rodenberg, J. Amend, A. Mozeika, E. Steltz, M. R. Zakin, H. Lipson, and H. M. Jaeger, "Universal robotic gripper based on the jamming of granular material," *Proceedings of the National Academy of Sciences*, vol. 107, no. 44, pp. 18 809–18 814, 2010.

[23] A. Jiang, G. Xynogalas, P. Dasgupta, K. Althoefer, and T. Nanayakkara, "Design of a variable stiffness flexible manipulator with composite granular jamming and membrane coupling," in *2012 IEEE/RSJ International Conference on Intelligent Robots and Systems*. IEEE, 2012, pp. 2922–2927.

[24] S. Follmer, D. Leithinger, A. Olwal, N. Cheng, and H. Ishii, "Jamming user interfaces: programmable particle stiffness and sensing for malleable and shape-changing devices," in *Proceedings of the 25th annual ACM symposium on User interface software and technology*. ACM, 2012, pp. 519–528.

[25] A. A. Stanley, J. C. Gwilliam, and A. M. Okamura, "Haptic jamming: A deformable geometry, variable stiffness tactile display using pneumatics and particle jamming," in *World Haptics Conference (WHC), 2013*. IEEE, 2013, pp. 25–30.

[26] M. Li, T. Ranzani, S. Sareh, L. D. Seneviratne, P. Dasgupta, H. A. Wurdemann, and K. Althoefer, "Multi-fingered haptic palpation utilizing granular jamming stiffness feedback actuators," *Smart Materials and Structures*, vol. 23, no. 9, p. 095007, 2014.

[27] I. Zubrycki and G. Granosik, "Novel haptic device using jamming principle for providing kinaesthetic feedback in glove-based control interface," *Journal of Intelligent & Robotic Systems*, pp. 1–17, 2016.

[28] Y.-J. Kim, S. Cheng, S. Kim, and K. Iagnemma, "A novel layer jamming mechanism with tunable stiffness capability for minimally invasive surgery," *IEEE Transactions on Robotics*, vol. 29, no. 4, pp. 1031–1042, 2013.

[29] T. M. Simon, R. T. Smith, and B. H. Thomas, "Wearable jamming mitten for virtual environment haptics," in *Proceedings of the 2014 ACM International Symposium on Wearable Computers*. ACM, 2014, pp. 67–70.

[30] T. M. Simon, B. H. Thomas, and R. T. Smith, "Low-profile jamming technology for medical rehabilitation," *IT Professional*, vol. 17, no. 5, pp. 28–34, 2015.

[31] J. Ou, L. Yao, D. Tauber, J. Steimle, R. Niiyama, and H. Ishii, "jamsheets: thin interfaces with tunable stiffness enabled by layer jamming," in *Proceedings of the 8th International Conference on Tangible, Embedded and Embodied Interaction*. ACM, 2014, pp. 65–72.

[32] V. Wall, R. Deimel, and O. Brock, "Selective stiffening of soft actuators based on jamming," in *2015 IEEE International Conference on Robotics and Automation (ICRA)*. IEEE, 2015, pp. 252–257.

[33] P. C. Mitiguy and A. K. Banerjee, "Efficient simulation of motions involving coulomb friction," *Journal of guidance, control, and dynamics*, vol. 22, no. 1, pp. 78–86, 1999.

[34] D. ASTM, "93: Standard test method for static and kinetic coefficients of friction of plastic film and sheeting," 1894.

[35] D. B. Camarillo, P. B. Shull, J. Mattson, R. Shultz, and D. Garza, "An instrumented mouthguard for measuring linear and angular head impact kinematics in american football," *Annals of biomedical engineering*, vol. 41, no. 9, pp. 1939–1949, 2013.

[36] S. Diller, C. Majidi, and S. H. Collins, "A lightweight, low-power electroadhesive clutch and spring for exoskeleton actuation," in *IEEE International Conference on Robotics and Automation*, 2016.

[37] T. Kikuchi, J. Furusho, and K. Oda, "Development of isokinetic exercise machine using er brake," in *Robotics and Automation, 2003. Proceedings. ICRA'03. IEEE International Conference on*, vol. 1. IEEE, 2003, pp. 214–219.

[38] M. Avraam, M. Horodinca, I. Romanescu, and A. Preumont, "Computer controlled rotational mr-brake for wrist rehabilitation device," *Journal of intelligent material systems and structures*, 2010.